Measurement of *b* hadron production fractions in 7 TeV *pp* collisions

R. Aaji *et al.**

(The LHCb Collaboration)

Measurements of *b* hadron production ratios in proton-proton collisions at a center-of-mass energy of 7 TeV with an integrated luminosity of 3 pb^{-1} are presented. We study the ratios of strange *B* meson to light *B* meson production $f_s/(f_u + f_d)$ and Λ_b^0 baryon to light *B* meson production $f_{\Lambda_b}/(f_u + f_d)$ as a function of the charmed hadron-muon pair transverse momentum p_T and the *b* hadron pseudorapidity η, for p_T between 0 and 14 GeV and η between 2 and 5. We find that $f_s/(f_u + f_d)$ is consistent with being independent of p_T and η, and we determine $f_s/(f_u + f_d) = 0.134 \pm 0.004^{+0.011}_{-0.010}$, where the first error is statistical and the second systematic. The corresponding ratio $f_{\Lambda_b}/(f_u + f_d)$ is found to be dependent upon the transverse momentum of the charmed hadron-muon pair, $f_{\Lambda_b}/(f_u + f_d) = (0.404 \pm 0.017(\text{stat}) \pm 0.027(\text{syst}) \pm 0.105(\text{Br})) \times [1 - (0.031 \pm 0.004(\text{stat}) \pm 0.003(\text{syst})) \times p_T(\text{GeV})]$, where Br reflects an absolute scale uncertainty due to the poorly known branching fraction $\mathcal{B}(\Lambda_c^+ \to pK^-\pi^+)$. We extract the ratio of strange *B* meson to light neutral *B* meson production f_s/f_d by averaging the result reported here with two previous measurements derived from the relative abundances of $\bar{B}_s^0 \to D_s^+\pi^-$ to $\bar{B}^0 \to D^+K^-$ and $\bar{B}^0 \to D^+\pi^-$. We obtain $f_s/f_d = 0.267^{+0.021}_{-0.020}$.

PACS numbers: 13.25.Hw, 14.20.Mr

I. INTRODUCTION

The fragmentation process, in which a primary *b* quark forms either a $b\bar{q}$ meson or a bq_1q_2 baryon, cannot be reliably predicted because it is driven by strong dynamics in the nonperturbative regime. Thus fragmentation functions for the various hadron species must be determined experimentally. The LHCb experiment at the LHC explores a unique kinematic region: it detects *b* hadrons produced in a cone centered around the beam axis covering a region of pseudorapidity η, defined in terms of the polar angle θ with respect to the beam direction as $-\ln(\tan\theta/2)$, ranging approximately between 2 and 5. Knowledge of the fragmentation functions allows us to relate theoretical predictions of the $b\bar{b}$ quark production cross-section, derived from perturbative QCD, to the observed hadrons. In addition, since many absolute branching fractions of B^- and $\bar{B}^0$ decays have been well measured at e^+e^- colliders [1], it suffices to measure the ratio of $\bar{B}_s^0$ production to either B^- or $\bar{B}^0$ production to perform precise absolute $\bar{B}_s^0$ branching fraction measurements. In this paper we describe measurements of two ratios of fragmentation functions: $f_s/(f_u + f_d)$ and $f_{\Lambda_b}/(f_u + f_d)$, where $f_q \equiv \mathcal{B}(b \to B_q)$ and $f_{\Lambda_b} \equiv \mathcal{B}(b \to \Lambda_b)$. The inclusion of charged conjugate modes is implied throughout the paper, and we measure the average production ratios.

Previous measurements of these fractions have been made at LEP [2] and at CDF [3]. More recently, LHCb

measured the ratio f_s/f_d using the decay modes $\bar{B}^0 \to D^+\pi^-$, $\bar{B}^0 \to D^+K^-$, and $\bar{B}_s^0 \to D_s^+\pi^-$ [4] and theoretical input from QCD factorization [5,6]. Here we measure this ratio using semileptonic decays without any significant model dependence. A commonly adopted assumption is that the fractions of these different species should be the same in high energy *b* jets originating from Z^0 decays and high p_T *b* jets originating from $p\bar{p}$ collisions at the Tevatron or pp collisions at LHC, based on the notion that hadronization is a nonperturbative process occurring at the scale of Λ_{QCD}. Nonetheless, the results from different experiments are discrepant in the case of the *b* baryon fraction [2].

The measurements reported in this paper are performed using the LHCb detector [7], a forward spectrometer designed to study production and decays of hadrons containing *b* or *c* quarks. LHCb includes a vertex detector (VELO), providing precise locations of primary *pp* interaction vertices, and of detached vertices of long-lived hadrons. The momenta of charged particles are determined using information from the VELO together with the rest of the tracking system, composed of a large area silicon tracker located before a 4 Tm dipole magnet, and a combination of silicon strip and straw drift chamber detectors located after the magnet. Two Ring Imaging Cherenkov (RICH) detectors are used for charged hadron identification. Photon detection and electron identification are implemented through an electromagnetic calorimeter followed by a hadron calorimeter. A system of alternating layers of iron and chambers provides muon identification. The two calorimeters and the muon system provide the energy and momentum information to implement a first level (L0) hardware trigger. An additional trigger level is software based, and its algorithms are tuned to the experiment's operating condition.

---

*Full author list given at the end of the article.

In this analysis we use a data sample of 3 pb^{-1} collected from 7 TeV center-of-mass energy pp collisions at the LHC during 2010. The trigger selects events where a single muon is detected without biasing the impact parameter distribution of the decay products of the b hadron, nor any kinematic variable relevant to semileptonic decays. These features reduce the systematic uncertainty in the efficiency. Our goal is to measure two specific production ratios: that of $\bar{B}_s^0$ relative to the sum of B^- and $\bar{B}^0$, and that of Λ_b^0, relative to the sum of B^- and $\bar{B}^0$. The sum of the $\bar{B}^0$, B^-, $\bar{B}_s^0$ and Λ_b^0 fractions does not equal one, as there is other b production, namely, a very small rate for B_c^- mesons, bottomonia, and other b baryons that do not decay strongly into Λ_b^0, such as the Ξ_b. We measure relative fractions by studying the final states $D^0\mu^-\bar{\nu}X$, $D^+\mu^-\bar{\nu}X$, $D_s^+\mu^-\bar{\nu}X$, $\Lambda_c^+\mu^-\bar{\nu}X$, $D^0K^+\mu^-\bar{\nu}X$, and $D^0p\mu^-\bar{\nu}X$. We do not attempt to separate f_u and f_d, but we measure the sum of D^0 and D^+ channels and correct for cross-feeds from $\bar{B}_s^0$ and Λ_b^0 decays. We assume near equality of the semileptonic decay width of all b hadrons, as discussed below. Charmed hadrons are reconstructed through the modes listed in Table I, together with their branching fractions. We use all $D_s^+ \to K^-K^+\pi^+$ decays rather than a combination of the resonant $\phi\pi^+$ and $\bar{K}^{*0}K^+$ contributions, because these D_s^+ decays cannot be cleanly isolated due to interference effects of different amplitudes.

Each of these different charmed hadron plus muon final states can be populated by a combination of initial b hadron states. $\bar{B}^0$ mesons decay semileptonically into a mixture of D^0 and D^+ mesons, while B^- mesons decay predominantly into D^0 mesons with a smaller admixture of D^+ mesons. Both include a tiny component of D_s^+K meson pairs. $\bar{B}_s^0$ mesons decay predominantly into D_s^+ mesons, but can also decay into D^0K^+ and $D^+K_S^0$ mesons; this is expected if the $\bar{B}_s^0$ decays into a D_s^{**} state that is heavy enough to decay into a DK pair. In this paper we measure this contribution using $D^0K^+X\mu^-\bar{\nu}$ events. Finally, Λ_b^0 baryons decay mostly into Λ_c^+ final states. We determine other contributions using $D^0pX\mu^-\bar{\nu}$ events. We ignore the contributions of $b \to u$ decays that comprise approximately 1% of semileptonic b hadron decays [10], and constitute a roughly equal portion of each b species in any case.

The corrected yields for $\bar{B}^0$ or B^- decaying into $D^0\mu^-\bar{\nu}X$ or $D^+\mu^-\bar{\nu}X$, $n_{\rm corr}$, can be expressed in terms of the measured yields, n, as

TABLE I. Charmed hadron decay modes and branching fractions.

Particle	Final state	Branching fraction (%)
D^0	$K^-\pi^+$	3.89 ± 0.05 [1]
D^+	$K^-\pi^+\pi^+$	9.14 ± 0.20 [8]
D_s^+	$K^-K^+\pi^+$	5.50 ± 0.27 [9]
Λ_c^+	$pK^-\pi^+$	5.0 ± 1.3 [1]

$$n_{\rm corr}(B \to D^0\mu) = \frac{1}{\mathcal{B}(D^0 \to K^-\pi^+)\epsilon(B \to D^0)}$$
$$\times \left[n(D^0\mu) - n(D^0K^+\mu)\frac{\epsilon(\bar{B}_s^0 \to D^0)}{\epsilon(\bar{B}_s^0 \to D^0K^+)} \right.$$
$$\left. - n(D^0p\mu)\frac{\epsilon(\Lambda_b^0 \to D^0)}{\epsilon(\Lambda_b^0 \to D^0p)} \right], \quad (1)$$

where we use the shorthand $n(D\mu) \equiv n(DX\mu^-\bar{\nu})$. An analogous abbreviation ϵ is used for the total trigger and detection efficiencies. For example, the ratio $\epsilon(\bar{B}_s^0 \to D^0)/\epsilon(\bar{B}_s^0 \to D^0K^+)$ gives the relative efficiency to reconstruct a charged K in semi-muonic $\bar{B}_s^0$ decays producing a D^0 meson. Similarly

$$n_{\rm corr}(B \to D^+\mu)$$
$$= \frac{1}{\epsilon(B \to D^+)}\left[\frac{n(D^+\mu^-)}{\mathcal{B}(D^+ \to K^-\pi^+\pi^+)} \right.$$
$$- \frac{n(D^0K^+\mu^-)}{\mathcal{B}(D^0 \to K^-\pi^+)}\frac{\epsilon(\bar{B}_s^0 \to D^+)}{\epsilon(\bar{B}_s^0 \to D^0K^+)}$$
$$\left. - \frac{n(D^0p\mu^-)}{\mathcal{B}(D^0 \to K^-\pi^+)}\frac{\epsilon(\Lambda b \to D^+)}{\epsilon(\Lambda b \to D^0p)} \right]. \quad (2)$$

Both the $D^0X\mu^-\bar{\nu}$ and the $D^+X\mu^-\bar{\nu}$ final states contain small components of cross-feed from $\bar{B}_s^0$ decays to $D^0K^+X\mu^-\bar{\nu}$ and to $D^+K^0X\mu^-\bar{\nu}$. These components are accounted for by the two decays $\bar{B}_s^0 \to D_{s1}^+X\mu^-\bar{\nu}$ and $\bar{B}_s^0 \to D_{s2}^{*+}X\mu^-\bar{\nu}$ as reported in a recent LHCb publication [11]. The third terms in Eqs. (1) and (2) are due to a similar small cross-feed from Λ_b^0 decays.

The number of $\bar{B}_s^0$ resulting in $D_s^+X\mu^-\bar{\nu}$ in the final state is given by

$$n_{\rm corr}(\bar{B}_s^0 \to D_s^+\mu) = \frac{1}{\epsilon(\bar{B}_s^0 \to D_s^+)}\left[\frac{n(D_s^+\mu)}{\mathcal{B}(D_s^+ \to K^+K^-\pi^+)} \right.$$
$$- N(\bar{B}^0 + B^-)\mathcal{B}(B \to D_s^+K\mu)$$
$$\left. \times \epsilon(\bar{B} \to D_s^+K\mu) \right], \quad (3)$$

where the last term subtracts yields of $D_s^+KX\mu^-\bar{\nu}$ final states originating from $\bar{B}^0$ or B^- semileptonic decays, and $N(\bar{B}^0 + B^-)$ indicates the total number of $\bar{B}^0$ and B^- produced. We derive this correction using the branching fraction $\mathcal{B}(B \to D_s^{(*)+}K\mu\nu) = (6.1 \pm 1.2) \times 10^{-4}$ [12] measured by the *BABAR* experiment. In addition, $\bar{B}_s^0$ decays semileptonically into $DKX\mu^-\bar{\nu}$, and thus we need to add to Eq. (3)

$$n_{\rm corr}(\bar{B}_s^0 \to DK\mu) = 2\frac{n(D^0K^+\mu)}{\mathcal{B}(D^0 \to K^-\pi^+)\epsilon(\bar{B}_s^0 \to D^0K^+\mu)}, \quad (4)$$

where, using isospin symmetry, the factor of 2 accounts for $\bar{B}_s^0 \to D\bar{K}^0X\mu^-\bar{\nu}$ semileptonic decays.

The equation for the ratio $f_s/(f_u + f_d)$ is

$$\frac{f_s}{f_u + f_d} = \frac{n_{\mathrm{corr}}(\bar{B}^0_s \to D\mu)}{n_{\mathrm{corr}}(B \to D^0\mu) + n_{\mathrm{corr}}(B \to D^+\mu)} \frac{\tau_{B^-} + \tau_{\bar{B}^0}}{2\tau_{\bar{B}^0_s}},$$
(5)

where $\bar{B}^0_s \to D\mu$ represents $\bar{B}^0_s$ semileptonic decays to a final charmed hadron, given by the sum of the contributions shown in Eqs. (3) and (4), and the symbols τ_{B_i} indicate the B_i hadron lifetimes, that are all well measured [1]. We use the average $\bar{B}^0_s$ lifetime, 1.472 ± 0.025 ps [1]. This equation assumes equality of the semileptonic widths of all the b meson species. This is a reliable assumption, as corrections in HQET arise only to order $1/m_b^2$ and the SU(3) breaking correction is quite small, of the order of 1% [13–15].

The Λ^0_b corrected yield is derived in an analogous manner. We determine

$$n_{\mathrm{corr}}(\Lambda^0_b \to D\mu) = \frac{n(\Lambda^+_c\mu^-)}{\mathcal{B}(\Lambda^+_c \to pK^-\pi^+)\epsilon(\Lambda^0_b \to \Lambda^+_c)} + 2\frac{n(D^0p\mu^-)}{\mathcal{B}(D^0 \to K^-\pi^+)\epsilon(\Lambda^0_b \to D^0p)},$$
(6)

where D represents a generic charmed hadron, and extract the Λ^0_b fraction using

$$\frac{f_{\Lambda_b}}{f_u + f_d} = \frac{n_{\mathrm{corr}}(\Lambda^0_b \to D\mu)}{n_{\mathrm{corr}}(B \to D^0\mu) + n_{\mathrm{corr}}(B \to D^+\mu)}$$
$$\times \frac{\tau_{B^-} + \tau_{\bar{B}^0}}{2\tau_{\Lambda^0_b}}(1 - \xi).$$
(7)

Again, we assume near equality of the semileptonic widths of different b hadrons, but we apply a small adjustment $\xi = 4 \pm 2\%$, to account for the chromomagnetic correction, affecting b-flavored mesons but not b baryons [13–15]. The uncertainty is evaluated with very conservative assumptions for all the parameters of the heavy quark expansion.

II. ANALYSIS METHOD

To isolate a sample of b flavored hadrons with low backgrounds, we match charmed hadron candidates with tracks identified as muons. Right-sign (RS) combinations have the sign of the charge of the muon being the same as the charge of the kaon in D^0, D^+, or Λ^+_c decays, or the opposite charge of the pion in D^+_s decays, while wrong-sign (WS) combinations comprise combinations with opposite charge correlations. WS events are useful to estimate certain backgrounds. This analysis follows our previous investigation of $b \to D^0 X\mu^-\bar{\nu}$ [16]. We consider events where a well-identified muon with momentum
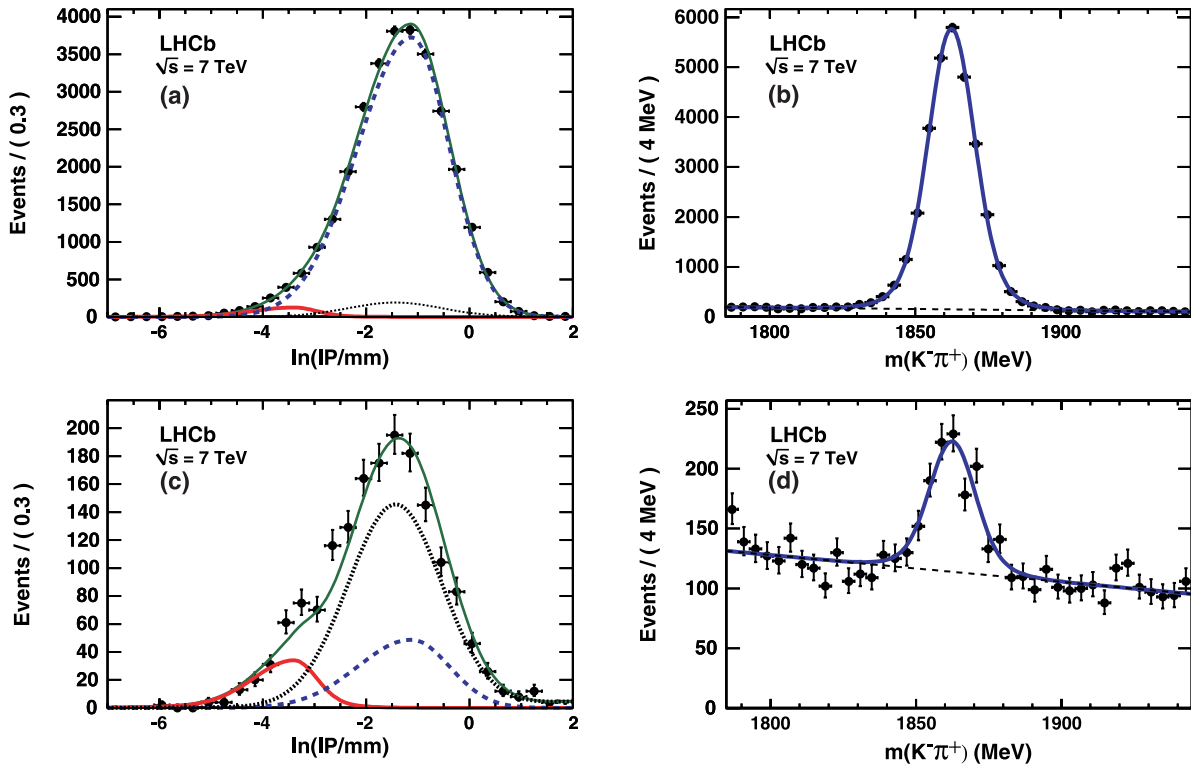

FIG. 1 (color online). The logarithm of the IP distributions for (a) RS and (c) WS D^0 candidate combinations with a muon. The dotted curves show the false D^0 background, the small red-solid curves the Prompt yields, the dashed curves the Dfb signal, and the larger green-solid curves the total yields. The invariant $K^-\pi^+$ mass spectra for (b) RS combinations and (d) WS combinations are also shown.

greater than 3 GeV and transverse momentum greater than 1.2 GeV is found. Charmed hadron candidates are formed from hadrons with momenta greater than 2 GeV and transverse momenta greater than 0.3 GeV, and we require that the average transverse momentum of the hadrons forming the candidate be greater than 0.7 GeV. Kaons, pions, and protons are identified using the RICH system. The impact parameter (IP), defined as the minimum distance of approach of the track with respect to the primary vertex, is used to select tracks coming from charm decays. We require that the χ^2, formed by using the hypothesis that each track's IP is equal to 0, is greater than 9. Moreover, the selected tracks must be consistent with coming from a common vertex: the χ^2 per number of degrees of freedom of the vertex fit must be smaller than 6. In order to ensure that the charm vertex is distinct from the primary pp interaction vertex, we require that the χ^2, based on the hypothesis that the decay flight distance from the primary vertex is zero, is greater than 100.

Charmed hadrons and muons are combined to form a partially reconstructed b hadron by requiring that they come from a common vertex, and that the cosine of the angle between the momentum of the charmed hadron and muon pair and the line from the $D\mu$ vertex to the primary

vertex be greater than 0.999. As the charmed hadron is a decay product of the b hadron, we require that the difference in z component of the decay vertex of the charmed hadron candidate and that of the beauty candidate be greater than 0. We explicitly require that the η of the b hadron candidate be between 2 and 5. We measure η using the line defined by connecting the primary event vertex and the vertex formed by the D and the μ. Finally, the invariant mass of the charmed hadron and muon system must be between 3 and 5 GeV for $D^0\mu^-$ and $D^+\mu^-$ candidates, between 3.1 and 5.1 GeV for $D_s^+\mu^-$ candidates, and between 3.3 and 5.3 GeV for $\Lambda_c^+\mu^-$ candidates.

We perform our analysis in a grid of 3 η and 5 p_T bins, covering the range $2 < \eta < 5$ and $p_T \leq 14$ GeV. The b hadron signal is separated from various sources of background by studying the two-dimensional distribution of charmed hadron candidate invariant mass and ln(IP/mm). This approach allows us to determine the background coming from false combinations under the charmed hadron signal mass peak directly. The study of the ln(IP/mm) distribution allows the separation of prompt charm decay candidates from charmed hadron daughters of b hadrons [16]. We refer to these samples as Prompt and Dfb, respectively.
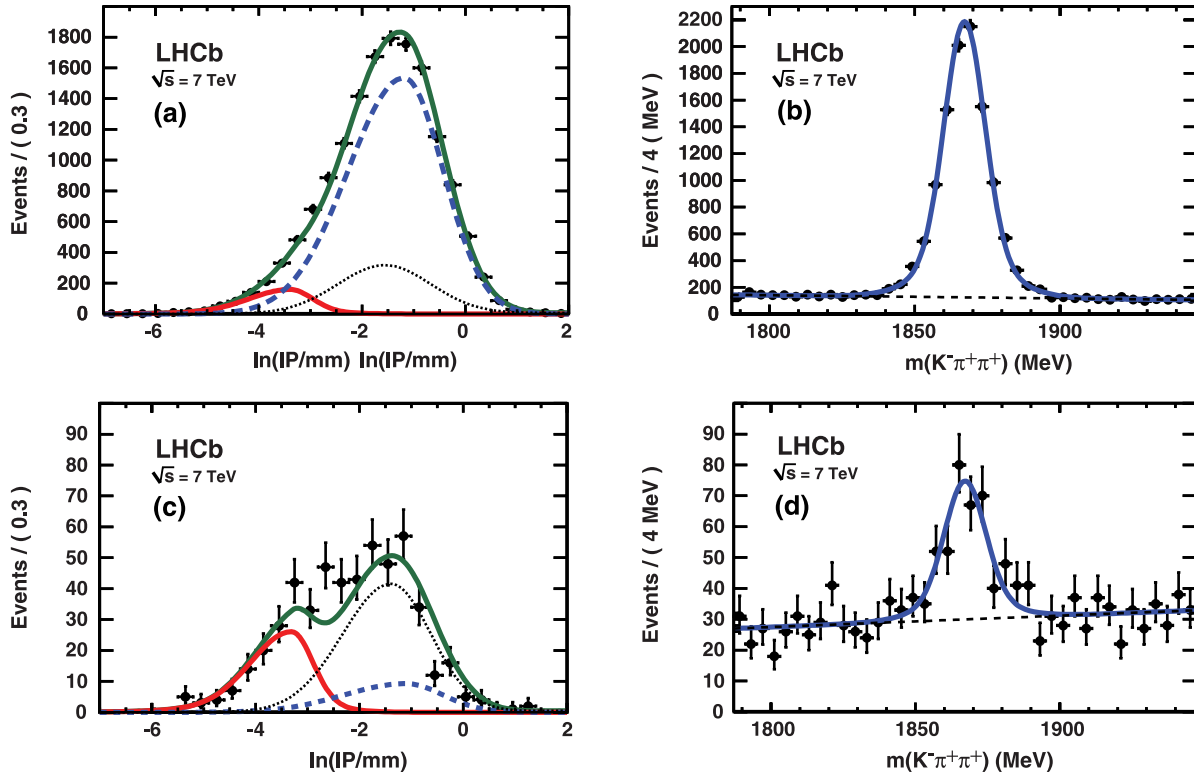

FIG. 2 (color online).   The logarithm of the IP distributions for (a) RS and (c) WS D^+ candidate combinations with a muon. The grey-dotted curves show the false D^+ background, the small red-solid curves the Prompt yields, the blue-dashed curves the Dfb signal, and the larger green-solid curves the total yields. The invariant $K^-\pi^+\pi^+$ mass spectra for (b) RS combinations and (d) WS combinations are also shown.

A. Signal extraction

We describe the method used to extract the charmed hadron-μ signal by using the $D^0 X \mu^- \bar{\nu}$ final state as an example; the same procedure is applied to the final states $D^+ X \mu^- \bar{\nu}$, $D_s^+ X \mu^- \bar{\nu}$, and $\Lambda_c^+ X \mu^- \bar{\nu}$. We perform unbinned extended maximum likelihood fits to the two-dimensional distributions in $K^- \pi^+$ invariant mass over a region extending ± 80 MeV from the D^0 mass peak, and ln (IP/mm). The parameters of the IP distribution of the Prompt sample are found by examining directly produced charm [16] whereas a shape derived from simulation is used for the Dfb component.

An example fit for $D^0 \mu^- \bar{\nu} X$, using the whole p_T and η range, is shown in Fig. 1. The fitted yields for RS are 27666 ± 187 Dfb, 695 ± 43 Prompt, and 1492 ± 30 false D^0 combinations, inferred from the fitted yields in the sideband mass regions, spanning the intervals between 35 and 75 MeV from the signal peak on both sides. For WS we find 362 ± 39 Dfb, 187 ± 18 Prompt, and 1134 ± 19 false D^0 combinations. The RS yield includes a background of around 0.5% from incorrectly identified μ candidates. As this paper focuses on ratios of yields, we do not subtract this component. Figure 2 shows the corresponding fits for the $D^+ X \mu^- \bar{\nu}$ final state. The fitted yields consist of 9257 ± 110 Dfb events, 362 ± 34 Prompt, and 1150 ± 22

false D^+ combinations. For WS we find 77 ± 22 Dfb, 139 ± 14 Prompt and 307 ± 10 false D^+ combinations.

The analysis for the $D_s^+ X \mu^- \bar{\nu}$ mode follows in the same manner. Here, however, we are concerned about the reflection from $\Lambda_c^+ \to p K^- \pi^+$ where the proton is taken to be a kaon, since we do not impose an explicit proton veto. Using such a veto would lose 30% of the signal and also introduce a systematic error. We choose to model separately this particular background. We add a probability density function (PDF) determined from simulation to model this, and the level is allowed to float within the estimated error on the size of the background. The small peak near 2010 MeV in Fig. 3(b) is due to $D^{*+} \to \pi^+ D^0$, $D^0 \to K^+ K^-$. We explicitly include this term in the fit, assuming the shape to be the same as for the D_s^+ signal, and we obtain 4 ± 1 events in the RS signal region and no events in the WS signal region. The measured yields in the RS sample are 2192 ± 64 Dfb, 63 ± 16 Prompt, 985 ± 145 false D_s^+ background, and 387 ± 132 Λ_c^+ reflection background. The corresponding yields in the WS sample are 13 ± 19, 20 ± 7, 499 ± 16, and 3 ± 3 respectively. Figure 3 shows the fit results.

The last final state considered is $\Lambda_c^+ X \mu^- \bar{\nu}$. Figure 4 shows the data and fit components to the ln(IP/mm) and $p K^- \pi^+$ invariant mass combinations for events with
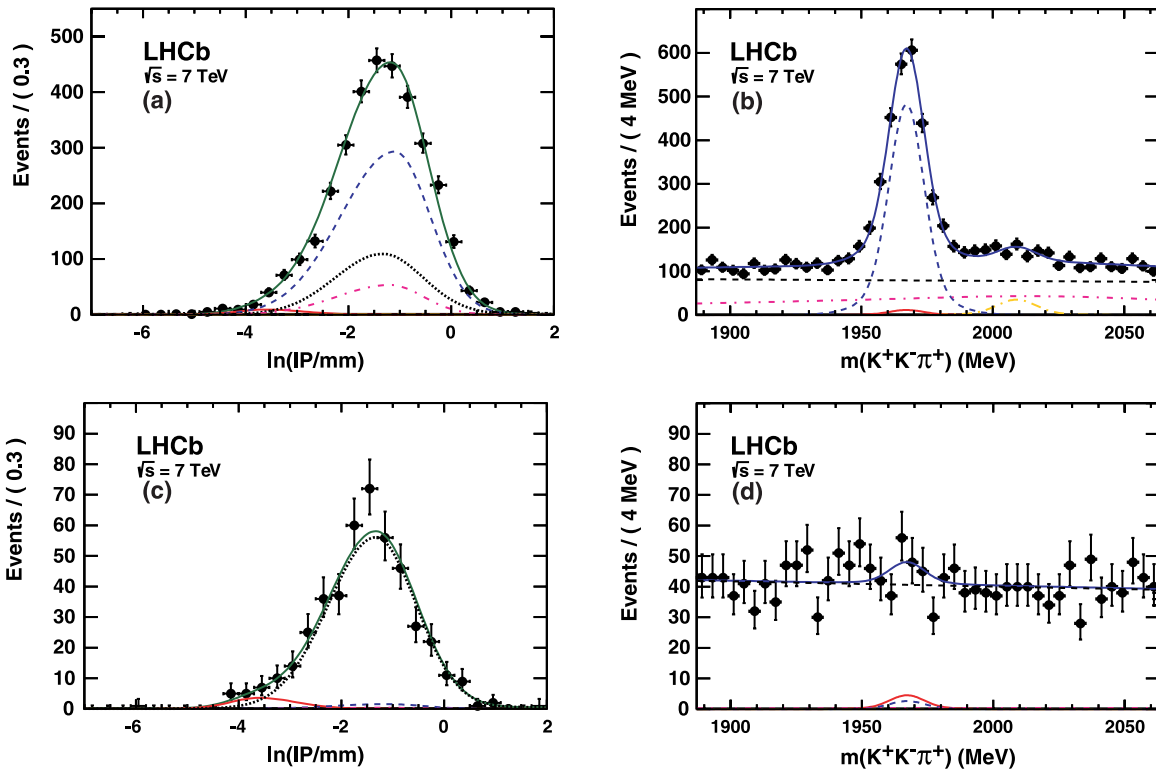

FIG. 3 (color online). The logarithm of the IP distributions for (a) RS and (c) WS D_s^+ candidate combinations with a muon. The grey-dotted curves show the false D_s^+ background, the small red-solid curves the Prompt yields, the blue-dashed curves the Dfb signal, the purple dash-dotted curves represent the background originating from Λ_c^+ reflection, and the larger green-solid curves the total yields. The invariant $K^- K^+ \pi^+$ mass spectra for RS combinations (b) and WS combinations (d) are also shown.
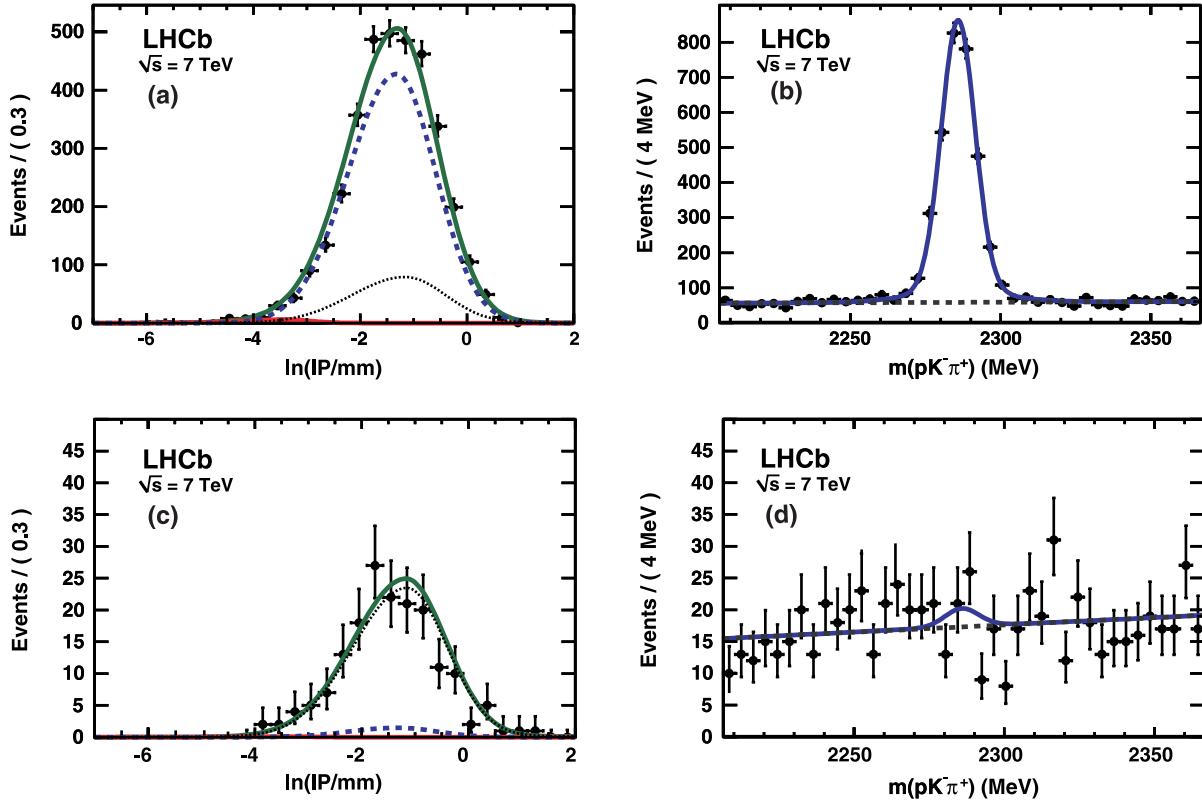
FIG. 4 (color online). The logarithm of the IP distributions for (a) RS and (c) WS Λ_c^+ candidate combinations with a muon. The grey-dotted curves show the false Λ_c^+ background, the small red-solid curves the Prompt yields, the blue-dashed curves the Dfb signal, and the larger green-solid curves the total yields. The invariant $pK^-\pi^+$ mass spectra for RS combinations (b) and WS combinations (d) are also shown.

$2 < \eta < 5$. This fit gives 3028 ± 112 RS Dfb events, 43 ± 17 RS Prompt events, 589 ± 27 RS false Λ_c^+ combinations, 9 ± 16 WS Dfb events, 0.5 ± 4 WS Prompt events, and 177 ± 10 WS false Λ_c^+ combinations.

The Λ_b^0 may also decay into $D^0 p X \mu^- \bar{\nu}$. We search for these decays by requiring the presence of a track well identified as a proton and detached from any primary vertex. The resulting $D^0 p$ invariant mass distribution is shown in Fig. 5. We also show the combinations that cannot arise from Λ_b^0 decay, namely, those with $D^0 \bar{p}$ combinations. There is a clear excess of RS over WS combinations especially near threshold. Fits to the $K^- \pi^+$ invariant mass in the $[m(K^- \pi^+ p) - m(K^- \pi^+) + m(D^0)_{\mathrm{PDG}}]$ region shown in Fig. 5(a) give 154 ± 13 RS events and 55 ± 8 WS events. In this case, we use the WS yield for background subtraction, scaled by the RS/WS background ratio determined with a MC simulation including $(B^- + \bar{B}^0 \rightarrow D^0 X \mu^- \bar{\nu})$ and generic $b\bar{b}$ events. This ratio is found to be 1.4 ± 0.2. Thus, the net signal is $76 \pm 17 \pm 11$, where the last error reflects the uncertainty in the ratio between RS and WS background.

B. Background studies

Apart from false D combinations, separated from the signal by the two-dimensional fit described above, there

are also physical background sources that affect the RS Dfb samples, and originate from $b\bar{b}$ events, which are studied with a MC simulation. In the meson case, the background mainly comes from $b \rightarrow DDX$ with one of the D mesons decaying semi-muonically, and from combinations of tracks from the $pp \rightarrow b\bar{b}X$ events, where one b hadron decays into a D meson and the other b hadron decays semi-muonically. The background fractions are $(1.9 \pm 0.3)\%$ for $D^0 X \mu^- \bar{\nu}$, $(2.5 \pm 0.6)\%$ for $D^+ X \mu^- \bar{\nu}$, and $(5.1 \pm 1.7)\%$ for $D_s^+ X \mu^- \bar{\nu}$. The main background component for Λ_b^0 semileptonic decays is Λ_b^0 decaying into $D_s^- \Lambda_c^+$, and the D_s^- decaying semi-muonically. Overall, we find a very small background rate of $(1.0 \pm 0.2)\%$, where the error reflects only the statistical uncertainty in the simulation. We correct the candidate b hadron yields in the signal region with the predicted background fractions. A conservative 3% systematic uncertainty in the background subtraction is assigned to reflect modelling uncertainties.

C. Monte Carlo simulation and efficiency determination

In order to estimate the detection efficiency, we need some knowledge of the different final states which contribute to the Cabibbo favored semileptonic width, as some of
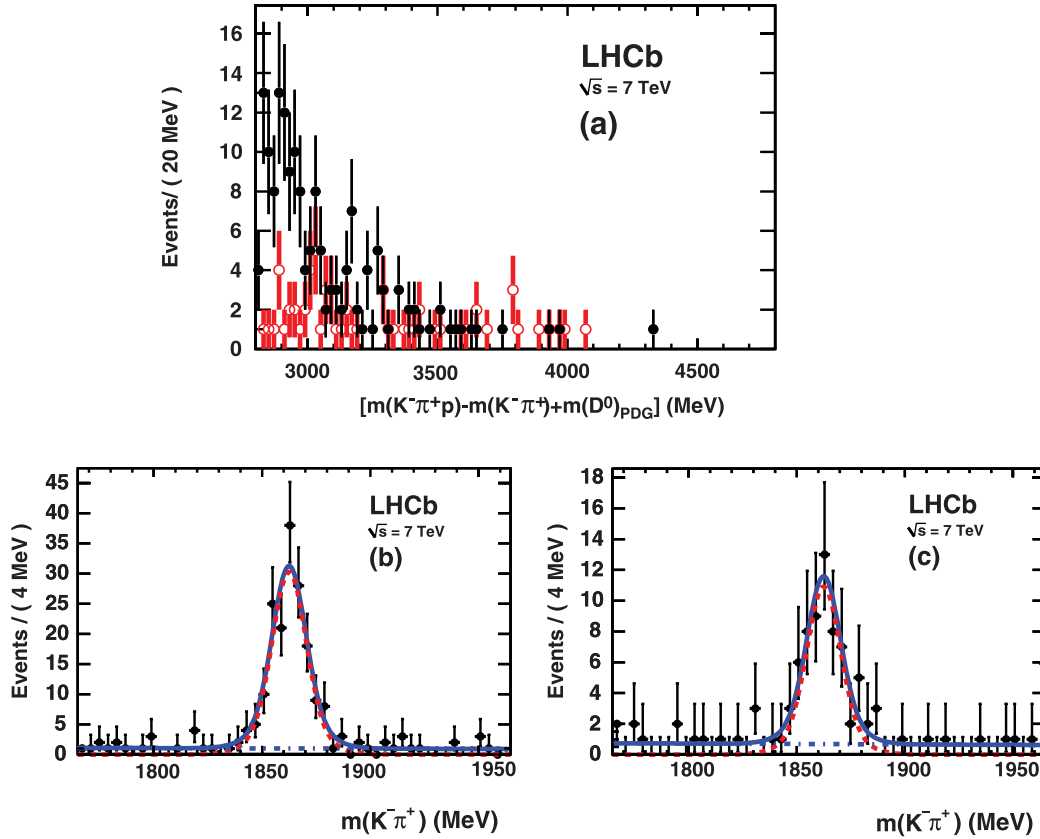
FIG. 5 (color online).   (a) Invariant mass of $D^0 p$ candidates that vertex with each other and together with a RS muon (black closed points) and for a $\bar{p}$ (red open points) instead of a p; (b) fit to D^0 invariant mass for RS events with the invariant mass of $D^0 p$ candidate in the signal mass difference window; (c) fit to D^0 invariant mass for WS events with the invariant mass of $D^0 p$ candidate in the signal mass difference window.

the selection criteria affect final states with distinct masses and quantum numbers differently. Although much is known about the $\bar{B}^0$ and B^- semileptonic decays, information on the corresponding $\bar{B}_s^0$ and Λ_b^0 semileptonic decays is rather sparse. In particular, the hadronic composition of the final states in $\bar{B}_s^0$ decays is poorly known [11], and only a study from CDF provides some constraints on the branching ratios of final states dominant in the corresponding Λ_b^0 decays [17].

In the case of the $\bar{B}_s^0 \to D_s^+$ semileptonic decays, we assume that the final states are D_s^+, D_s^{*+}, $D_{s0}^*(2317)^+$, $D_{s1}(2460)^+$, and $D_{s1}(2536)^+$. States above DK threshold decay predominantly into $D^{(*)}K$ final states. We model the decays to the final states $D_s^+ \mu^- \bar{\nu}$ and $D_s^{*+} \mu^- \bar{\nu}$ with HQET form factors using normalization coefficients derived from studies of the corresponding $\bar{B}^0$ and B^- semileptonic decays [1], while we use the ISGW2 form factor model [18] to describe final states including higher mass resonances.

In order to determine the ratio between the different hadron species in the final state, we use the measured kinematic distributions of the quasiexclusive process $\bar{B}_s^0 \to D_s^+ \mu^- \bar{\nu} X$. To reconstruct the squared invariant mass of the $\mu^- \bar{\nu}$ pair (q^2), we exploit the measured direction of the b

hadron momentum, which, together with energy and momentum conservation, assuming no missing particles other than the neutrino, allow the reconstruction of the ν 4-vector, up to a two-fold ambiguity, due to its unknown orientation with respect to the B flight path in its rest frame. We choose the solution corresponding to the lowest b hadron momentum. This method works well when there are no missing particles, or when the missing particles are soft, as in the case when the charmed system is a D^* meson. We then perform a two-dimensional fit to the q^2 versus $m(\mu D_s^+)$ distribution. Figure 6 shows stacked histograms of the D_s^+, D_s^{*+}, and D_s^{**+} components. In the fit we constrain the ratio $\mathcal{B}(\bar{B}_s^0 \to D_s^{*+} \mu^- \bar{\nu})/\mathcal{B}(\bar{B}_s^0 \to D_s^+ \mu^- \bar{\nu})$ to be equal to the average $D^* \mu^- \bar{\nu}/D \mu^- \bar{\nu}$ ratio in semileptonic $\bar{B}^0$ and B^- decays (2.42 ± 0.10) [1]. This constraint reduces the uncertainty of one D^{**} fraction. We have also performed fits removing this assumption, and the variation between the different components is used to assess the modelling systematic uncertainty.

A similar procedure is applied to the $\Lambda_c^+ \mu^-$ sample and the results are shown in Fig. 7. In this case we consider three final states, $\Lambda_c^+ \mu^- \bar{\nu}$, $\Lambda_c(2595)^+ \mu^- \bar{\nu}$, and $\Lambda_c(2625)^+ \mu^- \bar{\nu}$, with form factors from the model of
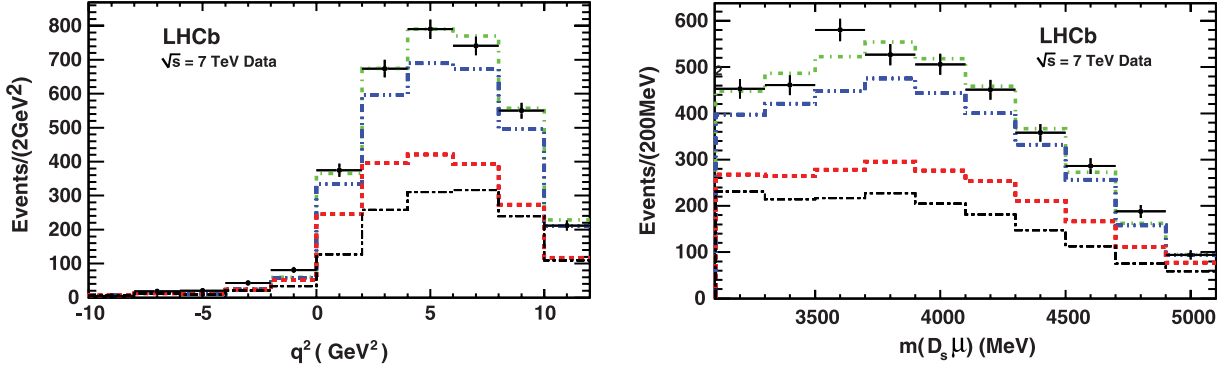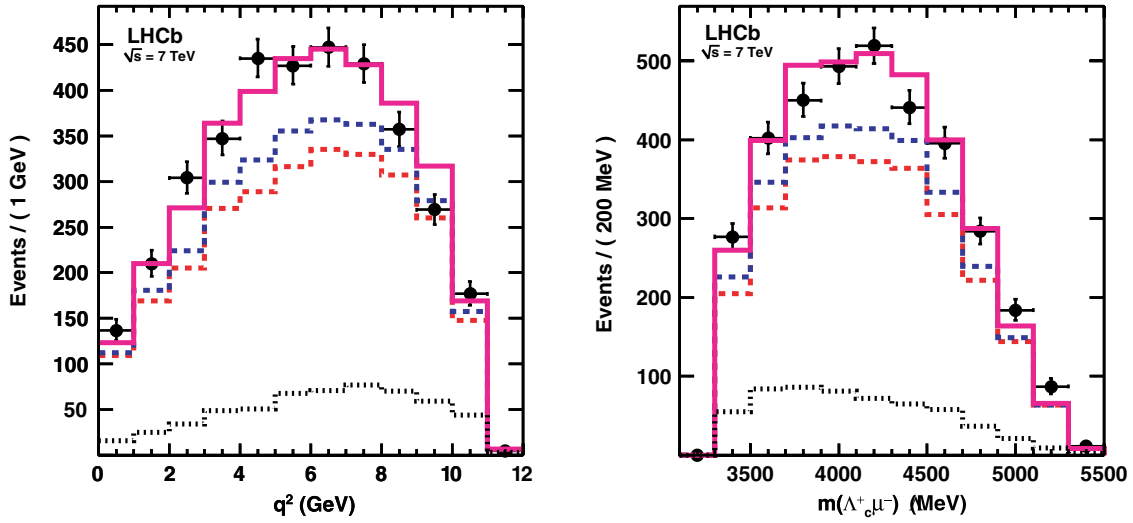
FIG. 6 (color online).   Projections of the two-dimensional fit to the q^2 and $m(D_s^+ \mu)$ distributions of semileptonic decays including a D_s^+ meson. The D_s^*/D_s ratio has been fixed to the measured D^*/D ratio in light B decays (2.42 ± 0.10), and the background contribution is obtained using the sidebands in the $K^+ K^- \pi^+$ mass spectrum. The different components are stacked: the background is represented by a black dot-dashed line, D_s^+ by a red dashed line, D_s^{*+} by a blue dash-double dotted line and D_s^{**+} by a green dash-dotted line.

FIG. 7 (color online).   Projections of the two-dimensional fit to the q^2 and $m(\Lambda_c^+ \mu^-)$ distributions of semileptonic decays including a Λ_c^+ baryon. The different components are stacked: the dotted line represents the combinatoric background, the bigger dashed line (red) represents the $\Lambda_c^+ \mu^- \bar{\nu}$ component, the smaller dashed line (blue) the $\Lambda_c(2595)^+$, and the solid line represents the $\Lambda_c(2625)^+$ component. The $\Lambda_c(2595)^+/\Lambda_c(2625)^+$ ratio is fixed to its predicted value, as described in the text.
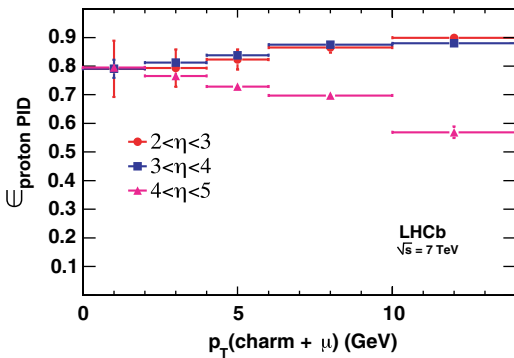
FIG. 8 (color online).   Measured proton identification efficiency as a function of the $\Lambda_c^+ \mu^-$ p_T for $2 < \eta < 3$, $3 < \eta < 4$, $4 < \eta < 5$ respectively, and for the selection criteria used in the $\Lambda_c^+ \to p K^- \pi^+$ reconstruction.

Ref. [19]. We constrain the two highest mass hadrons to be produced in the ratio predicted by this theory.

The measured pion, kaon, and proton identification efficiencies are determined using K_S^0, D^{*+}, and Λ^0 calibration samples where p, K, and π are selected without utilizing the particle identification criteria. The efficiency is obtained by fitting simultaneously the invariant mass distributions of events either passing or failing the identification requirements. Values are obtained in bins of the particle η and p_T, and these efficiency matrices are applied to the MC simulation. Alternatively, the particle identification efficiency can be determined by using the measured efficiencies and combining them with weights proportional to the fraction of particle types with a given η and p_T for each μ charmed hadron pair η and p_T bin. The overall efficiencies obtained with these two methods are consistent.
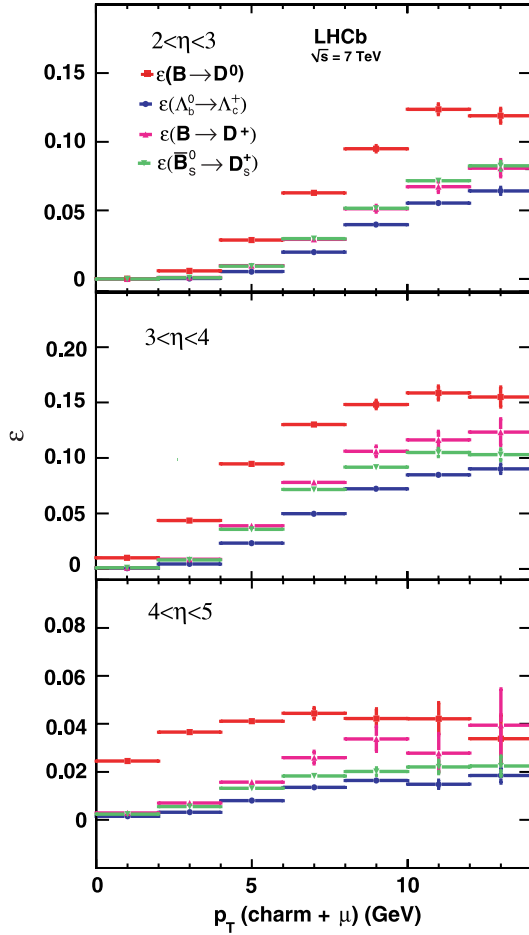
FIG. 9 (color online). Efficiencies for $D^0\mu^-\bar\nu X$, $D^+\mu^-\bar\nu X$, $D_s^+\mu^-\bar\nu X$, $\Lambda_c^+\mu^-\bar\nu X$ as a function of η and p_T.

An example of the resulting particle identification efficiency as a function of the η and p_T of the $\Lambda_c^+\mu^-$ pair is shown in Fig. 8.

As the functional forms of the fragmentation ratios in terms of p_T and η are not known, we determine the efficiencies for the final states studied as a function of p_T

and η within the LHCb acceptance. Figure 9 shows the results.

III. EVALUATION OF THE RATIOS $f_s/(f_u + f_d)$ AND $f_{\Lambda_b}/(f_u + f_d)$

Perturbative QCD calculations lead us to expect the ratios $f_s/(f_u + f_d)$ and $f_{\Lambda_b}/(f_u + f_d)$ to be independent of η, while a possible dependence upon the *b* hadron transverse momentum p_T is not ruled out, especially for ratios involving baryon species [20]. Thus we determine these fractions in different p_T and η bins. For simplicity, we use the transverse momentum of the charmed hadron-μ pair as the p_T variable, and do not try to unfold the *b* hadron transverse momentum.

In order to determine the corrected yields entering the ratio $f_s/(f_u + f_d)$, we determine yields in a matrix of three η and five p_T bins and divide them by the corresponding efficiencies. We then use Eq. (5), with the measured lifetime ratio $(\tau_{B^-} + \tau_{\bar B^0})/2\tau_{\bar B_s^0} = 1.07 \pm 0.02$ [1] to derive the ratio $f_s/(f_u + f_d)$ in two η bins. The measured ratio is constant over the whole η-p_T domain. Figure 10 shows the $f_s/(f_u + f_d)$ fractions in bins of p_T in two η intervals.

By fitting a single constant to all the data, we obtain $f_s/(f_u + f_d) = 0.134 \pm 0.004^{+0.011}_{-0.010}$ in the interval $2 < \eta < 5$, where the first error is statistical and the second is systematic. The latter includes several different sources listed in Table II. The dominant systematic uncertainty is caused by the experimental uncertainty on $\mathcal{B}(D_s^+ \to K^+K^-\pi^+)$ of 4.9%. Adding in the contributions of the D^0 and D^+ branching fractions we have a systematic error of 5.5% due to the charmed hadron branching fractions. The $\bar B_s^0$ semileptonic modelling error is derived by changing the ratio between different hadron species in the final state obtained by removing the SU(3) symmetry constrain, and changing the shapes of the less well known D^{**} states. The tracking efficiency errors mostly cancel in the ratio since we are dealing only with combinations of three or four tracks. The lifetime ratio error reflects the present experimental accuracy [1]. We correct both for the
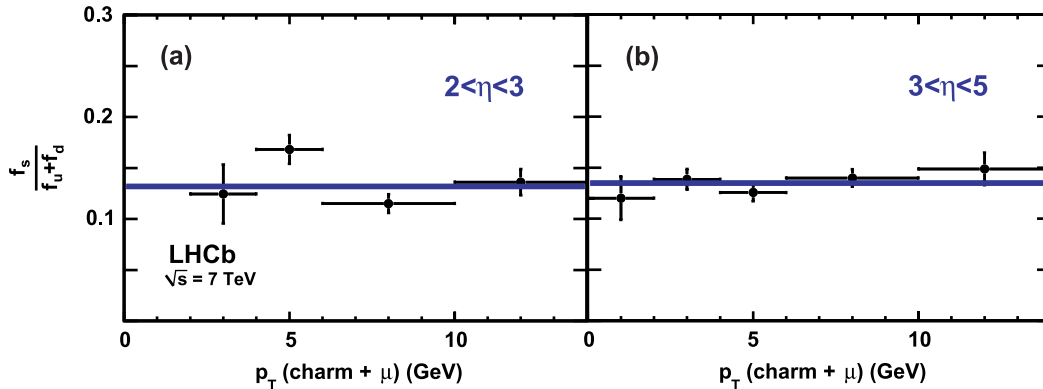

FIG. 10 (color online). Ratio between $\bar B_s^0$ and light *B* meson production fractions as a function of the transverse momentum of the $D_s^+\mu^-$ pair in two bins of η. The errors shown are statistical only.

TABLE II. Systematic uncertainties on the relative $\bar{B}_s^0$ production fraction.

Source	Error (%)
Bin-dependent errors	1.0
$\mathcal{B}(D^0 \to K^- \pi^+)$	1.2
$\mathcal{B}(D^+ \to K^- \pi^+ \pi^+)$	1.5
$\mathcal{B}(D_s^+ \to K^- K^+ \pi^+)$	4.9
$\bar{B}_s^0$ semileptonic decay modelling	3.0
Backgrounds	2.0
Tracking efficiency	2.0
Lifetime ratio	1.8
PID efficiency	1.5
$\bar{B}_s^0 \to D^0 K^+ X \mu^- \bar{\nu}$	$+4.1$ -1.1
$\mathcal{B}((B^-, \bar{B}^0) \to D_s^+ K X \mu^- \bar{\nu})$	2.0
Total	$+8.6$ -7.7

bin-dependent PID efficiency obtained with the procedure detailed before, accounting for the statistical error of the calibration sample, and the overall PID efficiency uncertainty, due to the sensitivity to the event multiplicity. The

latter is derived by taking the kaon identification efficiency obtained with the method described before, without correcting for the different track multiplicities in the calibration and signal samples. This is compared with the results of the same procedure performed correcting for the ratio of multiplicities in the two samples. The error due to $\bar{B}_s^0 \to D^0 K^+ X \mu^- \bar{\nu}$ is obtained by changing the RS/WS background ratio predicted by the simulation within errors, and evaluating the corresponding change in $f_s/(f_u + f_d)$. Finally, the error due to $(B^-, \bar{B}^0) \to D_s^+ K X \mu^- \bar{\nu}$ reflects the uncertainty in the measured branching fraction.

Isospin symmetry implies the equality of f_d and f_u, which allows us to compare $f_+/f_0 \equiv n_{\text{corr}}(D^+ \mu)/n_{\text{corr}}(D^0 \mu)$ with its expected value. It is not possible to decouple the two ratios for an independent determination of f_u/f_d. Using all the known semileptonic branching fractions [1], we estimate the expected relative fraction of the D^+ and D^0 modes from $B^{+/0}$ decays to be $f_+/f_0 = 0.375 \pm 0.023$, where the error includes a 6% theoretical uncertainty associated to the extrapolation of present experimental data needed to account for the inclusive
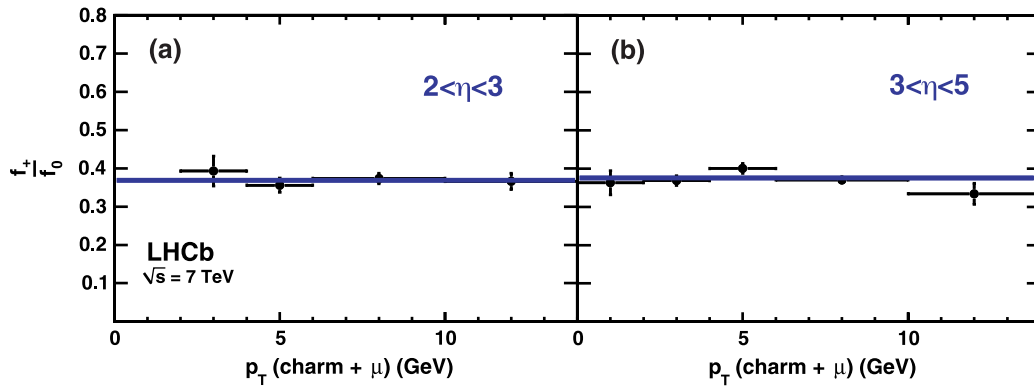

FIG. 11 (color online). f_+/f_0 as a function of p_{T} for $\eta = (2, 3)$ (a) and $\eta = (3, 5)$ (b). The horizontal line shows the average value. The error shown combines statistical and systematic uncertainties accounting for the detection efficiency and the particle identification efficiency.
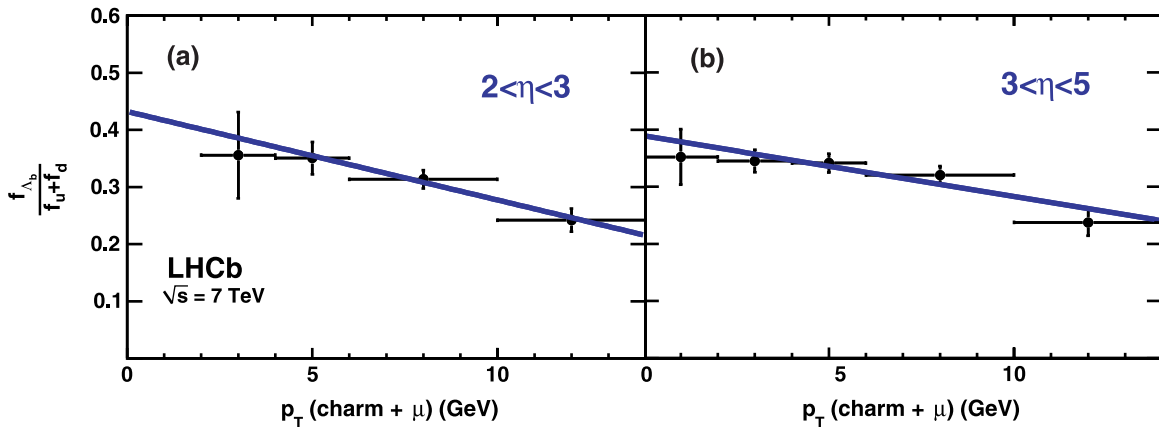

FIG. 12 (color online).   Fragmentation ratio $f_{\Lambda_b}/(f_u + f_d)$ dependence upon $p_{\text{T}}(\Lambda_c^+ \mu^-)$. The errors shown are statistical only.

$b \to c\mu^- \bar{\nu}$ semileptonic rate. Our corrected yields correspond to $f_+/f_0 = 0.373 \pm 0.006\,(\text{stat}) \pm 0.007\,(\text{eff}) \pm 0.014$, for a total uncertainty of 4.5%. The last error accounts for uncertainties in B background modelling, in the $D^0 K^+ \mu^- \bar{\nu}$ yield, the $D^0 p \mu^- \bar{\nu}$ yield, the D^0 and D^+ branching fractions, and tracking efficiency. The other systematic errors mostly cancel in the ratio. Our measurement of f_+/f_0 is not seen to be dependent upon p_T or η, as shown in Fig. 11, and is in agreement with expectation.

We follow the same procedure to derive the fraction $f_{\Lambda_b}/(f_u + f_d)$, using Eq. (7) and the ratio $(\tau_{B^-} + \tau_{\bar{B}^0})/(2\tau_{\Lambda_b^0}) = 1.14 \pm 0.03$ [1]. In this case, we observe a p_T dependence in the two η intervals. Figure 12 shows the data fitted to a straight line

$$\frac{f_{\Lambda_b}}{f_u + f_d} = a[1 + b \times p_T \text{ (GeV)}]. \qquad (8)$$

Table III summarizes the fit results. A corresponding fit to a constant shows that a p_T independent $f_{\Lambda_b}/(f_u + f_d)$ is excluded at the level of 4 standard deviations. The systematic errors reported in Table III include only the bin-dependent terms discussed above.

Table IV summarizes all the sources of absolute scale systematic uncertainties, that include several components. Their definitions mirror closely the corresponding

TABLE III. Coefficients of the linear fit describing the $p_T(\Lambda_c^+ \mu^-)$ dependence of $f_{\Lambda_b}/(f_u + f_d)$. The systematic uncertainties included are only those associated with the bin-dependent MC and particle identification errors.

η range	a	b
2–3	$0.434 \pm 0.040 \pm 0.025$	$-0.036 \pm 0.008 \pm 0.004$
3–5	$0.397 \pm 0.020 \pm 0.009$	$-0.028 \pm 0.006 \pm 0.003$
2–5	$0.404 \pm 0.017 \pm 0.009$	$-0.031 \pm 0.004 \pm 0.003$

TABLE IV. Systematic uncertainties on the absolute scale of $f_{\Lambda_b}/(f_u + f_d)$.

Source	Error (%)
Bin-dependent errors	2.2
$\mathcal{B}(\Lambda_b^0 \to D^0 p X \mu^- \bar{\nu})$	2.0
Monte Carlo modelling	1.0
Backgrounds	3.0
Tracking efficiency	2.0
Γ_{sl}	2.0
Lifetime ratio	2.6
PID efficiency	2.5
Subtotal	6.3
$\mathcal{B}(\Lambda_c^+ \to p K^- \pi^+)$	26.0
Total	26.8

uncertainties for the $f_s/(f_u + f_d)$ determination, and are assessed with the same procedures. The term $\Lambda_b \to D^0 p X \mu^- \bar{\nu}$ accounts for the uncertainty in the raw $D^0 p X \mu^- \bar{\nu}$ yield, and is evaluated by changing the RS/WS background ratio (1.4 ± 0.2) within the quoted uncertainty. In addition, an uncertainty of 2% is associated with the derivation of the semileptonic branching fraction ratios from the corresponding lifetimes, labeled Γ_{sl} in Table IV. The uncertainty is derived assigning conservative errors to the parameters affecting the chromomagnetic operator that influences the B meson total decay widths, but not the Λ_b^0. By far the largest term is the poorly known $\mathcal{B}(\Lambda_c^+ \to p K^- \pi^+)$; thus it is quoted separately.

In view of the observed dependence upon p_T, we present our results as

$$\left[\frac{f_{\Lambda_b}}{f_u + f_d}\right](p_T) = (0.404 \pm 0.017 \pm 0.027 \pm 0.105)$$
$$\times [1 - (0.031 \pm 0.004 \pm 0.003)$$
$$\times p_T \text{ (GeV)}], \qquad (9)$$

where the scale factor uncertainties are statistical, systematic, and the error on $\mathcal{B}(\Lambda_c \to p K^- \pi^+)$ respectively. The correlation coefficient between the scale factor and the slope parameter in the fit with the full error matrix is -0.63. Previous measurements of this fraction have been made at LEP and the Tevatron [3]. LEP obtains 0.110 ± 0.019 [2]. This fraction has been calculated by combining direct rate measurements with time-integrated mixing probability averaged over an unbiased sample of semileptonic b hadron decays. CDF measures $f_{\Lambda_b}/(f_u + f_d) = 0.281 \pm 0.012^{+0.011+0.128}_{-0.056-0.086}$, where the last error reflects the uncertainty in $\mathcal{B}(\Lambda_c^+ \to p K^- \pi^+)$. It has been suggested [3] that the difference between the Tevatron and LEP results is explained by the different kinematics of the two experiments. The average p_T of the $\Lambda_c^+ \mu^-$ system is 10 GeV for CDF, while the b-jets, at LEP, have $p \approx 40$ GeV. LHCb probes an even lower b p_T range, while retaining some sensitivity in the CDF kinematic region. These data are consistent with CDF in the kinematic region covered by both experiments, and indicate that the baryon fraction is higher in the lower p_T region.

IV. COMBINED RESULT FOR THE PRODUCTION FRACTION f_s/f_d FROM LHCB

From the study of b hadron semileptonic decays reported above, and assuming isospin symmetry, namely $f_u = f_d$, we obtain

$$\left(\frac{f_s}{f_d}\right)_{\text{sl}} = 0.268 \pm 0.008(\text{stat})^{+0.022}_{-0.020}(\text{syst}),$$

where the first error is statistical and the second is systematic.

Measurements of this quantity have also been made by LHCb by using hadronic B meson decays [4]. The ratio

TABLE V. Summary of the systematic and theoretical uncertainties in the three LHCb measurements of f_s/f_d.

Source	Error (%)			
	$(f_s/f_d)_{sl}$	$(f_s/f_d)_{h1}$	$(f_s/f_d)_{h2}$	
Bin-dependent error	1.0	$\cdots$	$\cdots$	Uncorrelated
Semileptonic decay modelling	3.0	$\cdots$	$\cdots$	Uncorrelated
Backgrounds	2.0	$\cdots$	$\cdots$	Uncorrelated
Fit model	$\cdots$	2.8	2.8	Uncorrelated
Trigger simulation	$\cdots$	2.0	2.0	Uncorrelated
Tracking efficiency	2.0	$\cdots$	$\cdots$	Uncorrelated
$\mathcal{B}(\bar{B}_s^0 \to D^0 K^+ X \mu^- \bar{\nu})$	$^{+4.1}_{-1.1}$	$\cdots$	$\cdots$	Uncorrelated
$\mathcal{B}(\bar{B}^0/B^- \to D_s^+ K X \mu^- \bar{\nu})$	2.0	$\cdots$	$\cdots$	Uncorrelated
Particle identification calibration	1.5	1.0	2.5	Correlated
B lifetimes	1.5	1.5	1.5	Correlated
$\mathcal{B}(D_s^+ \to K^+ K^- \pi^+)$	4.9	4.9	4.9	Correlated
$\mathcal{B}(D^+ \to K^- \pi^+ \pi^-)$	1.5	1.5	1.5	Correlated
SU(3) and form factors	$\cdots$	6.1	6.1	Correlated
W-exchange	$\cdots$	$\cdots$	7.8	Uncorrelated

determined using the relative abundances of $\bar{B}_s^0 \to D_s^+ \pi^-$ to $\bar{B}^0 \to D^+ K^-$ is

$$\left(\frac{f_s}{f_d}\right)_{h1} = 0.250 \pm 0.024(\text{stat}) \pm 0.017(\text{syst}) \pm 0.017(\text{theor}),$$

while that from the relative abundances of $\bar{B}_s^0 \to D_s^+ \pi^-$ to $\bar{B}^0 \to D^+ \pi^-$ [4] is

$$\left(\frac{f_s}{f_d}\right)_{h2} = 0.256 \pm 0.014(\text{stat}) \pm 0.019(\text{syst}) \pm 0.026(\text{theor}).$$

The first uncertainty is statistical, the second systematic and the third theoretical. The theoretical uncertainties in both cases include nonfactorizable SU(3)-breaking effects and form factor ratio uncertainties. The second ratio is affected by an additional source, accounting for the W-exchange diagram in the $\bar{B}^0 \to D^+ \pi^-$ decay.

In order to average these results, we consider the correlations between different sources of systematic uncertainties, as shown in Table V. We then utilize a generator of pseudoexperiments, where each independent source of uncertainty is generated as a random variable with

TABLE VI. Uncertainties in the combined value of f_s/f_d.

Source	Error (%)
Statistical	2.8
Experimental systematic (symmetric)	3.3
$\mathcal{B}(\bar{B}_s^0 \to D^0 K^+ X \mu^- \bar{\nu})$	$^{+3.0}_{-0.8}$
$\mathcal{B}(D^+ \to K^- \pi^+ \pi^-)$	2.2
$\mathcal{B}(D_s^+ \to K^+ K^- \pi^+)$	4.9
B lifetimes	1.5
$\mathcal{B}(\bar{B}^0/B^- \to D_s^+ K X \mu^- \bar{\nu})$	1.5
Theory	1.9

Gaussian distribution, except for the component $\bar{B}_s^0 \to D^0 K^+ \mu^- \bar{\nu}_\mu X$, which is modeled with a bifurcated Gaussian with standard deviations equal to the positive and negative errors shown in Table V. This approach to the averaging procedure is motivated by the goal of proper treatment of asymmetric errors [21]. We assume that the theoretical errors have a Gaussian distribution.

We define the average fraction as

$$f_s/f_d = \alpha_1 (f_s/f_d)_{sl} + \alpha_2 (f_s/f_d)_{h1} + \alpha_3 (f_s/f_d)_{h2}, \tag{10}$$

where

$$\alpha_1 + \alpha_2 + \alpha_3 = 1. \tag{11}$$

The RMS value of f_s/f_d is then evaluated as a function of α_1 and α_2.

We derive the most probable value f_s/f_d by determining the coefficients α_i at which the RMS is minimum, and the total errors by computing the boundaries defining the 68% CL, scanning from top to bottom along the axes α_1 and α_2 in the range comprised between 0 and 1. The optimal weights determined with this procedure are $\alpha_1 = 0.73$, and $\alpha_2 = 0.14$, corresponding to the most probable value

$$f_s/f_d = 0.267^{+0.021}_{-0.020}.$$

The most probable value differs slightly from a simple weighted average of the three measurements because of the asymmetry of the error distribution in the semileptonic determination. By switching off different components we can assess the contribution of each source of uncertainty. Table VI summarizes the results.

V. CONCLUSIONS

We measure the ratio of the $\bar{B}_s^0$ production fraction to the sum of those for B^- and $\bar{B}^0$ mesons $f_s/(f_u + f_d) = 0.134 \pm 0.004^{+0.011}_{-0.010}$, and find it consistent with being independent of η and p_T. Our results are more precise than, and in agreement with, previous measurements in different kinematic regions. We combine the LHCb measurements of the ratio of $\bar{B}_s^0$ to $\bar{B}^0$ production fractions obtained using *b* hadron semileptonic decays, and two different ratios of branching fraction of exclusive hadronic decays to derive $f_s/f_d = 0.267^{+0.021}_{-0.020}$. The ratio of the Λ_b^0 baryon production fraction to the sum of those for B^- and $\bar{B}^0$ mesons varies with the p_T of the charmed hadron-muon pair. Assuming a linear dependence up to $p_T = 14$ GeV, we obtain

$$\frac{f_{\Lambda_b}}{f_u + f_d} = (0.404 \pm 0.017 \pm 0.027 \pm 0.105)$$
$$\times [1 - (0.031 \pm 0.004 \pm 0.003) \times p_T \text{ (GeV)}],$$
$$(12)$$

where the errors on the absolute scale are statistical, systematic and error on $\mathcal{B}(\Lambda_c^+ \rightarrow pK^-\pi^+)$ respectively. No η dependence is found.

[1] K. Nakamura *et al.* Particle Data Group), J. Phys. G **37**, 075021 (2010).

[2] D. Asner *et al.* (Heavy Flavor Averaging Group), arXiv:1010.1589; online updates are available at http://www.slac.stanford.edu/xorg/hfag/osc/PDG_2010 2010.

[3] T. Aaltonen *et al.* (CDF collaboration), Phys. Rev. D **77**, 072003 (2008).

[4] R. Aaij *et al.* LHCb Collaboration), Phys. Rev. Lett. 107, 211801 (2011).

[5] R. Fleischer, N. Serra, and N. Tuning, Phys. Rev. D **82**, 034038 (2010).

[6] R. Fleischer, N. Serra, and N. Tuning, Phys. Rev. D **83**, 014017 (2011).

[7] A. Augusto Alves Jr. *et al.* (LHCb Collaboration), JINST **3**, S08005 (2008).

[8] S. Dobbs *et al.* (CLEO Collaboration), Phys. Rev. D **76**, 112001 (2007).

[9] J. Alexander *et al.* (CLEO Collaboration), Phys. Rev. Lett. **100**, 161804 (2008).

[10] M. Artuso, E. Barberio, and S. Stone, PMC Phys. A **3**, 3 (2009).

[11] R. Aaij *et al.* (LHCb Collaboration), Phys. Lett. B **698**, 14 (2011).

[12] P. del Amo Sanchez *et al.* (*BABAR* Collaboration), Phys. Rev. Lett. **107**, 041804 (2011).

[13] A. V. Manohar and M. B. Wise, Phys. Rev. D **49**, 1310 (1994).

[14] I. I. Y. Bigi, M. A. Shifman, N. G. Uraltsev, and A. I. Vainshtein, Phys. Rev. Lett. **71**, 496 (1993).

[15] I. I Bigi, T. Mannel, and N. Uraltsev, J. High Energy Phys. 09 (2011) 012.

[16] R. Aaij *et al.* LHCb Collaboration), Phys. Lett. B **694**, 209 (2010).

[17] T Aaltonen *et al.* (CDF Collaboration), Phys. Rev. D **79**, 032001 (2009).

[18] D. Scora and N. Isgur, Phys. Rev. D **52**, 2783 (1995).

[19] M. Pervin, W. Roberts, and S. Capstick, Phys. Rev. C **72**, 035201 (2005).

[20] M. Mangano, talk given at *Charm and Bottom Quark Production at the LHC* (CERN, Geneva, 2010).

[21] R. Barlow, arXiv:physics/0406120v1.

R. Aaji,[23] C. Abellan Beteta,[35,a] B. Adeva,[36] M. Adinolfi,[42] C. Adrover,[6] A. Affolder,[48] Z. Ajaltouni,[5] J. Albrecht,[37] F. Alessio,[37] M. Alexander,[47] G. Alkhazov,[29] P. Alvarez Cartelle,[36] A. A. Alves Jr,[22] S. Amato,[2] Y. Amhis,[38] J. Anderson,[39] R. B. Appleby,[50] O. Aquines Gutierrez,[10] F. Archilli,[18,37] L. Arrabito,[53] A. Artamonov,[34] M. Artuso,[52,37] E. Aslanides,[6] G. Auriemma,[22,b] S. Bachmann,[11] J. J. Back,[44] D. S. Bailey,[50] V. Balagura,[30,37] W. Baldini,[16] R. J. Barlow,[50] C. Barschel,[37] S. Barsuk,[7] W. Barter,[43] A. Bates,[47] C. Bauer,[10] Th. Bauer,[23] A. Bay,[38]

I. Bediaga,[1] K. Belous,[34] I. Belyaev,[30,37] E. Ben-Haim,[8] M. Benayoun,[8] G. Bencivenni,[18] S. Benson,[46] J. Benton,[42] R. Bernet,[39] M.-O. Bettler,[17] M. van Beuzekom,[23] A. Bien,[11] S. Bifani,[12] A. Bizzeti,[17,c] P. M. Bjørnstad,[50] T. Blake,[37] F. Blanc,[38] C. Blanks,[49] J. Blouw,[11] S. Blusk,[52] A. Bobrov,[33] V. Bocci,[22] A. Bondar,[33] N. Bondar,[29] W. Bonivento,[15] S. Borghi,[47] A. Borgia,[52] T. J. V. Bowcock,[48] C. Bozzi,[16] T. Brambach,[9] J. van den Brand,[24] J. Bressieux,[38] D. Brett,[50] S. Brisbane,[51] M. Britsch,[10] T. Britton,[52] N. H. Brook,[42] H. Brown,[48] A. Büchler-Germann,[39] I. Burducea,[28] A. Bursche,[39] J. Buytaert,[37] S. Cadeddu,[15] J. M. Caicedo Carvajal,[37] O. Callot,[7] M. Calvi,[20,d] M. Calvo Gomez,[35,a] A. Camboni,[35] P. Campana,[18,37] A. Carbone,[14] G. Carboni,[21,e] R. Cardinale,[19,37,f] A. Cardini,[15] L. Carson,[36] K. Carvalho Akiba,[2] G. Casse,[48] M. Cattaneo,[37] M. Charles,[51] Ph. Charpentier,[37] N. Chiapolini,[39] K. Ciba,[37] X. Cid Vidal,[36] G. Ciezarek,[49] P. E. L. Clarke,[46,37] M. Clemencic,[37] H. V. Cliff,[43] J. Closier,[37] C. Coca,[28] V. Coco,[23] J. Cogan,[6] P. Collins,[37] A. Comerma-Montells,[35] F. Constantin,[28] G. Conti,[38] A. Contu,[51] A. Cook,[42] M. Coombes,[42] G. Corti,[37] G. A. Cowan,[38] R. Currie,[46] B. D'Almagne,[7] C. D'Ambrosio,[37] P. David,[8] I. De Bonis,[4] S. De Capua,[21,e] M. De Cian,[39] F. De Lorenzi,[12] J. M. De Miranda,[1] L. De Paula,[2] P. De Simone,[18] D. Decamp,[4] M. Deckenhoff,[9] H. Degaudenzi,[38,37] M. Deissenroth,[11] L. Del Buono,[8] C. Deplano,[15] D. Derkach,[14,37] O. Deschamps,[5] F. Dettori,[24] J. Dickens,[43] H. Dijkstra,[37] P. Diniz Batista,[1] F. Domingo Bonal,[35,a] S. Donleavy,[48] F. Dordei,[11] A. Dosil Suárez,[36] D. Dossett,[44] A. Dovbnya,[40] F. Dupertuis,[38] R. Dzhelyadin,[34] S. Easo,[45] U. Egede,[49] V. Egorychev,[30] S. Eidelman,[33] D. van Eijk,[23] F. Eisele,[11] S. Eisenhardt,[46] R. Ekelhof,[9] L. Eklund,[47] Ch. Elsasser,[39] D. Esperante Pereira,[36] L. Estève,[43] A. Falabella,[16,g] E. Fanchini,[20,d] C. Färber,[11] G. Fardell,[46] C. Farinelli,[23] S. Farry,[12] V. Fave,[38] V. Fernandez Albor,[36] M. Ferro-Luzzi,[37] S. Filippov,[32] C. Fitzpatrick,[46] M. Fontana,[10] F. Fontanelli,[19,f] R. Forty,[37] M. Frank,[37] C. Frei,[37] M. Frosini,[17,37,h] S. Furcas,[20] A. Gallas Torreira,[36] D. Galli,[14,i] M. Gandelman,[2] P. Gandini,[51] Y. Gao,[3] J-C. Garnier,[37] J. Garofoli,[52] J. Garra Tico,[43] L. Garrido,[35] D. Gascon,[35] C. Gaspar,[37] N. Gauvin,[38] M. Gersabeck,[37] T. Gershon,[44,37] Ph. Ghez,[4] V. Gibson,[43] V. V. Gligorov,[37] C. Göbel,[54] D. Golubkov,[30] A. Golutvin,[49,30,37] A. Gomes,[2] H. Gordon,[51] M. Grabalosa Gándara,[35] R. Graciani Diaz,[35] L. A. Granado Cardoso,[37] E. Graugés,[35] G. Graziani,[17] A. Grecu,[28] E. Greening,[51] S. Gregson,[43] B. Gui,[52] E. Gushchin,[32] Yu. Guz,[34] T. Gys,[37] G. Haefeli,[38] C. Haen,[37] S. C. Haines,[43] T. Hampson,[42] S. Hansmann-Menzemer,[11] R. Harji,[49] N. Harnew,[51] J. Harrison,[50] P. F. Harrison,[44] J. He,[7] V. Heijne,[23] K. Hennessy,[48] P. Henrard,[5] J. A. Hernando Morata,[36] E. van Herwijnen,[37] E. Hicks,[48] K. Holubyev,[11] P. Hopchev,[4] W. Hulsbergen,[23] P. Hunt,[51] T. Huse,[48] R. S. Huston,[12] D. Hutchcroft,[48] D. Hynds,[47] V. Iakovenko,[41] P. Ilten,[12] J. Imong,[42] R. Jacobsson,[37] A. Jaeger,[11] M. Jahjah Hussein,[5] E. Jans,[23] F. Jansen,[23] P. Jaton,[38] B. Jean-Marie,[7] F. Jing,[3] M. John,[51] D. Johnson,[51] C. R. Jones,[43] B. Jost,[37] M. Kaballo,[9] S. Kandybei,[40] M. Karacson,[37] T. M. Karbach,[9] J. Keaveney,[12] U. Kerzel,[37] T. Ketel,[24] A. Keune,[38] B. Khanji,[6] Y. M. Kim,[46] M. Knecht,[38] P. Koppenburg,[23] A. Kozlinskiy,[23] L. Kravchuk,[32] K. Kreplin,[11] M. Kreps,[44] G. Krocker,[11] P. Krokovny,[11] F. Kruse,[9] K. Kruzelecki,[37] M. Kucharczyk,[20,25,37] S. Kukulak,[25] R. Kumar,[14,37] T. Kvaratskheliya,[30,37] V. N. La Thi,[38] D. Lacarrere,[37] G. Lafferty,[50] A. Lai,[15] D. Lambert,[46] R. W. Lambert,[37] E. Lanciotti,[37] G. Lanfranchi,[18] C. Langenbruch,[11] T. Latham,[44] R. Le Gac,[6] J. van Leerdam,[23] J.-P. Lees,[4] R. Lefèvre,[5] A. Leflat,[31,37] J. Lefrançois,[7] O. Leroy,[6] T. Lesiak,[25] L. Li,[3] L. Li Gioi,[5] M. Lieng,[9] M. Liles,[48] R. Lindner,[37] C. Linn,[11] B. Liu,[3] G. Liu,[37] J. H. Lopes,[2] E. Lopez Asamar,[35] N. Lopez-March,[38] J. Luisier,[38] F. Machefert,[7] I. V. Machikhiliyan,[4,30] F. Maciuc,[10] O. Maev,[29,37] J. Magnin,[1] S. Malde,[51] R. M. D. Mamunur,[37] G. Manca,[15,j] G. Mancinelli,[6] N. Mangiafave,[43] U. Marconi,[14] R. Märki,[38] J. Marks,[11] G. Martellotti,[22] A. Martens,[7] L. Martin,[51] A. Martín Sánchez,[7] D. Martinez Santos,[37] A. Massafferri,[1] Z. Mathe,[12] C. Matteuzzi,[20] M. Matveev,[29] E. Maurice,[6] B. Maynard,[52] A. Mazurov,[16,32,37] G. McGregor,[50] R. McNulty,[12] C. Mclean,[14] M. Meissner,[11] M. Merk,[23] J. Merkel,[9] R. Messi,[21,e] S. Miglioranzi,[37] D. A. Milanes,[13,37] M.-N. Minard,[4] S. Monteil,[5] D. Moran,[12] P. Morawski,[25] R. Mountain,[52] I. Mous,[23] F. Muheim,[46] K. Müller,[39] R. Muresan,[28,38] B. Muryn,[26] M. Musy,[35] J. Mylroie-Smith,[48] P. Naik,[42] T. Nakada,[38] R. Nandakumar,[45] I. Nasteva,[1] M. Nedos,[9] M. Needham,[46] N. Neufeld,[37] C. Nguyen-Mau,[38,k] M. Nicol,[7] V. Niess,[5] N. Nikitin,[31] A. Nomerotski,[51] A. Novoselov,[34] A. Oblakowska-Mucha,[26] V. Obraztsov,[34] S. Oggero,[23] S. Ogilvy,[47] O. Okhrimenko,[41] R. Oldeman,[15,j] M. Orlandea,[28] J. M. Otalora Goicochea,[2] P. Owen,[49] K. Pal,[52] J. Palacios,[39] A. Palano,[13,l] M. Palutan,[18] J. Panman,[37] A. Papanestis,[45] M. Pappagallo,[13,l] C. Parkes,[47,37] C. J. Parkinson,[49] G. Passaleva,[17] G. D. Patel,[48] M. Patel,[49] S. K. Paterson,[49] G. N. Patrick,[45] C. Patrignani,[19,f] C. Pavel-Nicorescu,[28] A. Pazos Alvarez,[36] A. Pellegrino,[23] G. Penso,[22,m] M. Pepe Altarelli,[37] S. Perazzini,[14,i] D. L. Perego,[20,d] E. Perez Trigo,[36] A. Pérez-Calero Yzquierdo,[35] P. Perret,[5] M. Perrin-Terrin,[6] G. Pessina,[20] A. Petrella,[16,37] A. Petrolini,[19,f] E. Picatoste Olloqui,[35] B. Pie Valls,[35] B. Pietrzyk,[4] T. Pilar,[44] D. Pinci,[22] R. Plackett,[47] S. Playfer,[46] M. Plo Casasus,[36] G. Polok,[25] A. Poluektov,[44,33] E. Polycarpo,[2] D. Popov,[10] B. Popovici,[28] C. Potterat,[35] A. Powell,[51] T. du Pree,[23] J. Prisciandaro,[38] V. Pugatch,[41]

A. Puig Navarro,[35] W. Qian,[52] J. H. Rademacker,[42] B. Rakotomiaramanana,[38] M. S. Rangel,[2] I. Raniuk,[40] G. Raven,[24] S. Redford,[51] M. M. Reid,[44] A. C. dos Reis,[1] S. Ricciardi,[45] K. Rinnert,[48] D. A. Roa Romero,[5] P. Robbe,[7] E. Rodrigues,[47] F. Rodrigues,[2] P. Rodriguez Perez,[36] G. J. Rogers,[43] S. Roiser,[37] V. Romanovsky,[34] M. Rosello,[35,a] J. Rouvinet,[38] T. Ruf,[37] H. Ruiz,[35] G. Sabatino,[21,e] J. J. Saborido Silva,[36] N. Sagidova,[29] P. Sail,[47] B. Saitta,[15,j] C. Salzmann,[39] M. Sannino,[19,f] R. Santacesaria,[22] C. Santamarina Rios,[36] R. Santinelli,[37] E. Santovetti,[21,e] M. Sapunov,[6] A. Sarti,[18,m] C. Satriano,[22,b] A. Satta,[21] M. Savrie,[16,g] D. Savrina,[30] P. Schaack,[49] M. Schiller,[24] S. Schleich,[9] M. Schmelling,[10] B. Schmidt,[37] O. Schneider,[38] A. Schopper,[37] M.-H. Schune,[7] R. Schwemmer,[37] B. Sciascia,[18] A. Sciubba,[18,m] M. Seco,[36] A. Semennikov,[30] K. Senderowska,[26] I. Sepp,[49] N. Serra,[39] J. Serrano,[6] P. Seyfert,[11] B. Shao,[3] M. Shapkin,[34] I. Shapoval,[40,37] P. Shatalov,[30] Y. Shcheglov,[29] T. Shears,[48] L. Shekhtman,[33] O. Shevchenko,[40] V. Shevchenko,[30] A. Shires,[49] R. Silva Coutinho,[54] H. P. Skottowe,[43] T. Skwarnicki,[52] A. C. Smith,[37] N. A. Smith,[48] E. Smith,[51,45] K. Sobczak,[5] F. J. P. Soler,[47] A. Solomin,[42] F. Soomro,[49] B. Souza De Paula,[2] B. Spaan,[9] A. Sparkes,[46] P. Spradlin,[47] F. Stagni,[37] S. Stahl,[11] O. Steinkamp,[39] S. Stoica,[28] S. Stone,[52,37] B. Storaci,[23] M. Straticiuc,[28] U. Straumann,[39] N. Styles,[46] V. K. Subbiah,[37] S. Swientek,[9] M. Szczekowski,[27] P. Szczypka,[38] T. Szumlak,[26] S. T'Jampens,[4] E. Teodorescu,[28] F. Teubert,[37] E. Thomas,[37] J. van Tilburg,[11] V. Tisserand,[4] M. Tobin,[39] S. Topp-Joergensen,[51] N. Torr,[51] E. Tournefier,[4,49] M. T. Tran,[38] A. Tsaregorodtsev,[6] N. Tuning,[23] M. Ubeda Garcia,[37] A. Ukleja,[27] P. Urquijo,[52] U. Uwer,[11] V. Vagnoni,[14] G. Valenti,[14] R. Vazquez Gomez,[35] P. Vazquez Regueiro,[36] S. Vecchi,[16] J. J. Velthuis,[42] M. Veltri,[17,n] K. Vervink,[37] B. Viaud,[7] I. Videau,[7] X. Vilasis-Cardona,[35,a] J. Visniakov,[36] A. Vollhardt,[39] D. Voong,[42] A. Vorobyev,[29] H. Voss,[10] S. Wandernoth,[11] J. Wang,[52] D. R. Ward,[43] A. D. Webber,[50] D. Websdale,[49] M. Whitehead,[44] D. Wiedner,[11] L. Wiggers,[23] G. Wilkinson,[51] M. P. Williams,[44,45] M. Williams,[49] F. F. Wilson,[45] J. Wishahi,[9] M. Witek,[25] W. Witzeling,[37] S. A. Wotton,[43] K. Wyllie,[37] Y. Xie,[46] F. Xing,[51] Z. Xing,[52] Z. Yang,[3] R. Young,[46] O. Yushchenko,[34] M. Zavertyaev,[10,o] F. Zhang,[3] L. Zhang,[52] W. C. Zhang,[12] Y. Zhang,[3] A. Zhelezov,[11] L. Zhong,[3] E. Zverev,[31] and A. Zvyagin[37]

(The LHCb Collaboration)

[1]*Centro Brasileiro de Pesquisas Físicas (CBPF), Rio de Janeiro, Brazil*
[2]*Universidade Federal do Rio de Janeiro (UFRJ), Rio de Janeiro, Brazil*
[3]*Center for High Energy Physics, Tsinghua University, Beijing, China*
[4]*LAPP, Université de Savoie, CNRS/IN2P3, Annecy-Le-Vieux, France*
[5]*Clermont Université, Université Blaise Pascal, CNRS/IN2P3, LPC, Clermont-Ferrand, France*
[6]*CPPM, Aix-Marseille Université, CNRS/IN2P3, Marseille, France*
[7]*LAL, , USAUniversité Paris-Sud, CNRS/IN2P3, Orsay, France*
[8]*LPNHE, , USAUniversité Pierre et Marie Curie, Université Paris Diderot, CNRS/IN2P3, Paris, France*
[9]*Fakultät Physik, Technische Universität Dortmund, Dortmund, Germany*
[10]*Max-Planck-Institut für Kernphysik (MPIK), Heidelberg, Germany*
[11]*Physikalisches Institut, Ruprecht-Karls-Universität Heidelberg, Heidelberg, Germany*
[12]*School of Physics, University College Dublin, Dublin, Ireland*
[13]*Sezione INFN di Bari, Bari, Italy*
[14]*Sezione INFN di Bologna, Bologna, Italy*
[15]*Sezione INFN di Cagliari, Cagliari, Italy*
[16]*Sezione INFN di Ferrara, Ferrara, Italy*
[17]*Sezione INFN di Firenze, Firenze, Italy*
[18]*Laboratori Nazionali dell'INFN di Frascati, Frascati, Italy*
[19]*Sezione INFN di Genova, Genova, Italy*
[20]*Sezione INFN di Milano Bicocca, Milano, Italy*
[21]*Sezione INFN di Roma Tor Vergata, Roma, Italy*
[22]*Sezione INFN di Roma La Sapienza, Roma, Italy*
[23]*Nikhef National Institute for Subatomic Physics, Amsterdam, Netherlands*
[24]*Nikhef National Institute for Subatomic Physics and Vrije Universiteit, Amsterdam, Netherlands*
[25]*Henryk Niewodniczanski Institute of Nuclear Physics Polish Academy of Sciences, Cracow, Poland*
[26]*Faculty of Physics & Applied Computer Science, Cracow, Poland*
[27]*Soltan Institute for Nuclear Studies, Warsaw, Poland*
[28]*Horia Hulubei National Institute of Physics and Nuclear Engineering, Bucharest-Magurele, Romania*
[29]*Petersburg Nuclear Physics Institute (PNPI), Gatchina, Russia*
[30]*Institute of Theoretical and Experimental Physics (ITEP), Moscow, Russia*

[31]*Institute of Nuclear Physics, Moscow State University (SINP MSU), Moscow, Russia*
[32]*Institute for Nuclear Research of the Russian Academy of Sciences (INR RAN), Moscow, Russia*
[33]*Budker Institute of Nuclear Physics (SB RAS) and Novosibirsk State University, Novosibirsk, Russia*
[34]*Institute for High Energy Physics (IHEP), Protvino, Russia*
[35]*Universitat de Barcelona, Barcelona, Spain*
[36]*Universidad de Santiago de Compostela, Santiago de Compostela, Spain*
[37]*European Organization for Nuclear Research (CERN), Geneva, Switzerland*
[38]*Ecole Polytechnique Fédérale de Lausanne (EPFL), Lausanne, Switzerland*
[39]*Physik-Institut, Universität Zürich, Zürich, Switzerland*
[40]*NSC Kharkiv Institute of Physics and Technology (NSC KIPT), Kharkiv, Ukraine*
[41]*Institute for Nuclear Research of the National Academy of Sciences (KINR), Kyiv, Ukraine*
[42]*H. H. Wills Physics Laboratory, University of Bristol, Bristol, United Kingdom*
[43]*Cavendish Laboratory, University of Cambridge, Cambridge, United Kingdom*
[44]*Department of Physics, University of Warwick, Coventry, United Kingdom*
[45]*STFC Rutherford Appleton Laboratory, Didcot, United Kingdom*
[46]*School of Physics and Astronomy, University of Edinburgh, Edinburgh, United Kingdom*
[47]*School of Physics and Astronomy, University of Glasgow, Glasgow, United Kingdom*
[48]*Oliver Lodge Laboratory, University of Liverpool, Liverpool, United Kingdom*
[49]*Imperial College London, London, United Kingdom*
[50]*School of Physics and Astronomy, University of Manchester, Manchester, United Kingdom*
[51]*Department of Physics, University of Oxford, Oxford, United Kingdom*
[52]*Syracuse University, Syracuse, New York, United States, USA*
[53]*CC-IN2P3, CNRS/IN2P3, Lyon-Villeurbanne, France, associated member*
[54]*Pontifícia Universidade Católica do Rio de Janeiro (PUC-Rio), Rio de Janeiro, Brazil,*
associated to Universidade Federal do Rio de Janeiro (UFRJ), Rio de Janeiro, Brazil

[a]LIFAELS, La Salle, Universitat Ramon Llull, Barcelona, Spain
[b]Università della Basilicata, Potenza, Italy
[c]Università di Modena e Reggio Emilia, Modena, Italy
[d]Università di Milano Bicocca, Milano, Italy
[e]Università di Roma Tor Vergata, Roma, Italy
[f]Università di Genova, Genova, Italy
[g]Università di Ferrara, Ferrara, Italy
[h]Università di Firenze, Firenze, Italy
[i]Università di Bologna, Bologna, Italy
[j]Università di Cagliari, Cagliari, Italy
[k]Hanoi University of Science, Hanoi, Vietnam
[l]Università di Bari, Bari, Italy
[m]Università di Roma La Sapienza, Roma, Italy
[n]Università di Urbino, Urbino, Italy
[o]P. N. Lebedev Physical Institute, Russian Academy of Science (LPI RAS), Moscow, Russia